Chapter 6

Mapping and Monitoring Wetland Dynamics Using Thermal, Optical, and SAR Remote Sensing Data

Gordana Kaplan, Zehra Yigit Avdan and Ugur Avdan

Additional information is available at the end of the chapter

http://dx.doi.org/10.5772/intechopen.80264

Abstract

Wetlands are transition zone where the flow of water, the cycling of carbon and nutrients, and the energy to form a unique ecosystem are characterized by its hydrology, soils, and vegetation, between dryland and water. Over the years, remote sensing techniques have proven to be a successful tool for monitoring wetlands. Both optical and microwave earth observation sensors can be used for monitoring wetlands. Land surface temperature (LST), as one of the most important variables in physical processes of the Earth, is one of the unexplored parameters for studying wetland dynamics. In this chapter, seasonal LST, SAR data values (dual polarization VV + VH), as well as the seasonal normalized difference water index will be explored, and the relation between them will be analyzed. For this purpose, satellite images from Landsat 8 and Sentinel-1, over a wetland area, were downloaded, preprocessed, and analyzed. As a study case, Seyfe Lake located in the central Anatolian part of Turkey has been selected. The results show Seyfe Lake's seasonal dynamics and the relation between the investigated parameters. The results helped in understanding the wetland seasonal dynamics which can be used in better managing and monitoring wetlands using remote sensing data.

Keywords: wetlands, remote sensing, land surface temperature, Landsat, synthetic aperture radar, normalized difference water index

1. Introduction

As one of the most productive natural ecosystems, wetlands are of great significant importance for hydrological and ecological processes. Wetlands have remarkable features in the landscape, which provide numerous beneficial services for people, fish, and wildlife. Wetlands can be

defined as areas filled or soaked with water at least for one part of the year. The complex hydrology of wetlands controls the source, amount, and temporal and spatial distribution of sediment and nutrient movements and influences the distribution of flora and fauna [1]. Over the past decades, threats like global climate change, and land-use conversion, arise the vulnerability of wetlands, and it is known that since the 1900s, the loss of wetlands has gained considerable attention with more than 50%. Thus, a need for continuous monitoring of the wetlands and their behavior is crucial for their protection and sustainable management. Remote sensing techniques are often less costly and time-consuming for large geographic areas compared to conventional field mapping [2] and have been a successful tool for monitoring wetlands in the past few decades.

1.1. A short review on remote sensing for wetland mapping and monitoring

Over the past few decades, remote sensing technology has been the most effective tool to acquire both spatial and temporal wetlands data. Remote sensing data has been used in a number of wetland research areas such as mapping wetland changes [3–5], carbon cycle and climate warming in wetland environments [6], and hydrology dynamics in wetlands [4]. A recent review of wetland remote sensing [7] states that the number of wetland remote sensing publication has drastically risen since the 1990s. In the same review, the contribution of medium spatial resolution data for wetland studies is elaborated. Both optical and microwave earth observation sensors can be used for monitoring wetlands; thus, optical satellites are mostly effective in vegetation monitoring as well as the wetlands' change mapping [8]. However, data from optical satellites have been used for mapping surface wetland water using different techniques that applied range in complexity and general applicability [9–11].

Synthetic aperture radar (SAR) technology provides significantly important data with its ability to image landscape through cloud cover, day and night, which often can be a limitation for optical sensors. Over the years, SAR data have been successfully used in different land-use/land cover applications. Recently, the European Space Agency launched two twin SAR satellites in order to continue the ERS and Envisat missions, Sentinel-1A and Sentinel-1B. The satellites carry a C-band (∼5.7 cm wavelength) SAR instrument offering data products in single (HH or VV) or double (HH + VH or VV + VH) polarization. With the launch of the Sentinel-1 mission, a new era for SAR mapping has begun; thus, the use of C-band in monitoring changes and mapping wetlands has increased. Research cover is not limited to the following topics: mapping and characterization of hydrological dynamics [12], short-term change detection in wetlands [13], assessment of carbon flux and soil moisture in wetlands [14], as well as a combination of Sentinel-1 and Sentinel-2 data for wetland classification [15]. The relation between radar and optical/thermal data can be significant for better understanding and managing wetlands. Several studies have investigated the relation between different satellite data in different land covers [16]. However, the relation between SAR values and land surface temperature values within a wetland area has not been a subject of a delicate investigation.

Land surface temperature (LST) is one of the most important variables in physical processes of the Earth, and it is one of the unexplored parameters for studying wetland dynamics [17]. LST is closely related to the surface energy balance and the water status of the land cover, and it

http://dx.doi.org/10.5772/intechopen.80264

depends on the radiative energy that the land absorbs [18]. With the latest technological developments in remote sensing, many Earth observation satellites like Landsat, Sentinel-3, MODIS, and ASTER operate in the thermal infrared region offering thermal bands for retrieving thermal maps of the Earth's surface. Landsat 8 is the latest satellite from the Landsat legacy, and it offers 100-m thermal data. Retrieving LST using Landsat data has been the subject in many studies resulting in several methods and algorithms [19, 20]. LST from satellite images has been used in different studies such as studies related to urban heat islands [21], earthquake monitoring [22], water extraction [23], climate changes, etc. One of the important parameters to understand the extensive range of existing processes in the wetland areas is the LST [24].

Normalized difference water index (NDWI) is one of the several indices commonly used in wetland studies [7]. The first remote sensing water index developed in 1995 is similar to the simplicity of the normalized difference vegetation index (NDVI); the NDWI uses two narrow channels centered near 0.86 and 1.24 μm or near the infrared and the short-wave infrared band which measures the liquid water molecules in [25] vegetation canopies that have interacted with solar radiation. Afterward, new water index developed to extract open water features using the green and the near-infrared band was proposed [26] and later modified by applying short-wave infrared instead of the near-infrared [27]. However, the use of short-wave infrared for water bodies' extraction within a wetland area is preferable, particularly in the presence of high level of suspended sediment. The NDWI product varies between −1 and +1 and depends on the water content in the observed area. Higher values correspond to high water content. NDWI values higher than zero are considered to be open water areas, while values close to zero are considered to be contents with high moisture.

The goal of this chapter is to present the seasonal wetland dynamics using SAR data values from Sentinel-1, LST data, as well as modified normalized difference water index (MNDWI) values retrieved from Landsat 8 compared with field measurements. Also, the relation between these significant parameters will be investigated and discussed.

1.2. Landsat 8 data

Starting from 1972, the Landsat program is the longest Earth observation platform. The most recent satellite, Landsat 8, has been launched in February 2013. Over the years, the Landsat data as a valuable resource for global research has been used in different applications. Landsat 8 carries two instruments, operational land imager (OLI) and thermal infrared sensor (TIRS). OLI collects data from nine, while TIRS collects data from two spectral bands (**Table 1**).

Taking into consideration the complex construction of wetland as a transition between terrestrial and open water aquatic ecosystems [28], wetlands and their properties are not easily detectable with optical satellite sensors [29]. However, wetlands are more sensitive to some parts of the electromagnetic spectrum than others. Thus, the near-infrared is sensitive to biomass content, in combination with the green band, and can give valuable information for the water content, as well as for the soil wetness [30]. On the other hand, the short-wave infrared bands are more sensitive to a moisture content of both soil and vegetation, and they are particularly useful in separating wetland from dry lands.

Spectral band	Wavelength (μm)	Resolution (m)
Band 1—Coastal/Aerosol	0.433–0.453	30
Band 2—Blue	0.450–0.515	30
Band 3—Green	0.525–0.600	30
Band 4—Red	0.630–680	30
Band 5—NIR	0.845–0.885	30
Band 6—SWIR-1	1.560–1660	30
Band 7—SWIR-2	2.100–2.300	30
Band 8—Panchromatic	0.500–0.680	15
Band 9—Cirrus	1.360–1.390	30
Band 10—LWIR-1	10.30–11.30	100
Band 11—LWIR-2	11.50–12.50	100

Table 1. Landsat 8 band specification.

As a follower of the Landsat 8 mission, the upcoming Landsat 9 which is expected to be launched in 2021 will continue to observe the Earth and collect valuable data for researchers all over the world.

1.3. Sentinel-1 data

The latest SAR satellite developed by the European Space Agency, Sentinel-1, is an imaging radar satellite at C-band (5.405 GHz) consisting of a constellation of two satellites, Sentinel-1A, launched on 3 April, 2014, and Sentinel-1B, launched on 22 April 2016. The C-SAR instruments support the operation of dual polarization: HH + HV and VV + VH. Their main cover applications are monitoring sea ice zones and the Arctic environment; surveillance of marine environment; mentoring land surface motion risks; mapping of land surfaces like forest, water, and soil and agriculture; and mapping in support of humanitarian aid on crisis situation [31, 32].

As a result of a number of environmental circumstances and system factors, satellite images can be often distorted in geometry and brightness which requires preprocessing of the images before their use [33]. SAR data are exposed to radiometric and geometric distortions that should be removed or minimized. The preprocessing of the Sentinel-1 SAR data can be easily done with the Sentinel-1 Toolbox integrated in SNAP, and it contains few steps: (i) data preparation, (ii) radiometric calibration, (iii) multilooking, (iv) spackle reduction, (v) terrain correction, and (vi) dB conversion.

The data preparation consists of selecting the study area, selecting the data type needed for the study, selecting the date, and downloading the SAR product.

Radiometric calibration corrects the SAR image so that the pixel values represent the radar backscatter of the reflected surface. SAR calibration provides imagery in which the pixel values can be directly related to the radar backscatter of the scene.

http://dx.doi.org/10.5772/intechopen.80264

Multilooking processing is used in order to produce a product with nominal image pixel size [34]. Multilooks can be generated by averaging over the range and/or azimuth resolution cells which improves the radiometric resolution but degrades the spatial resolution of the SAR image. Multilooking can be an optional processing since it is not necessary when terrain correction is applied to an image.

Compared to optical image data, the biggest difference in the appearance of radar imagery is its poor radiometric quality [33]; thus, it is difficult to make a visual interpretation of a SAR image. Speckle can be caused by random constructive and destructive interference resulting in salt and pepper noise over the SAR image [34]. As speckle is one of the biggest noises in SAR data, it should be reduced before performing any analyses.

Terrain correction geocodes the image by correcting SAR geometric distortions with the help of digital elevation model (DEM), and it produces a map projected product. With geocoding the image is being converted from slant range or ground range geometry into a map coordinate system. Terrain correction corrects SAR geometry effects such as foreshortening, layover, and shadows.

The last step of the preprocessing of Sentinel-1 SAR image is to convert the image in decibel scaling which can be done automatically in SNAP with right-click on the terrain-corrected image and selection of the linear to/from dB option (Eq. (1)):

$$\sigma^{\circ}\,\mathrm{dB} = 10\ \log_{10}\left(\sigma^{\circ}\right) \tag{1}$$

where $\sigma^{\circ}dB$ is sigma nought in decibel scale and σ° is the radiometric calibrated/speckle-reducted/terrain-corrected Level-1 SAR product.

2. Case study

In order to investigate wetlands' condition and seasonal changes, in this chapter, we review case study of thermal, optical, and radar remote sensing data and their relation for better understanding of wetland dynamics. As a study area, Seyfe Lake, located in the central Anatolian region, has been selected (**Figure 1**).

2.1. Study area

Turkey is the richest country in wetlands among Europe and the Middle East countries and with its geographical location plays an important part in the migration path for water birds. Seyfe Lake is located in the central Anatolian region, or 200 km northeast from Turkey's capital Ankara and 30 km east from Kirsehir. Seyfe Lake is a salty internal lake formed the base of a closed catchment area in a tectonic pit covering area approximately 10,700 ha. Over the years over 186 different bird species have been observed. Seyfe Lake is a first-degree natural site area under the protection of natural structure and ecological character pledged by the Ramsar Agreement in 1994. The lake is surrounded with agricultural areas, and according to the field

Figure 1. 14 June 2018, Seyfe Lake.

Figure 2. Seyfe Lake, June 1987 (left) and June 2018 (right).

observation on 14 June 2018, most of the agricultural fields around the lake are wheat, barley, and chickpeas.

This internationally valuable wetland area has been losing its value over the years. As seen in **Figure 2**, the water area has drastically decreased since 1987.

2.2. Data and methods

Satellite images from both Landsat 8 and Sentinel-1 satellites were used for observing the seasonal changes in Seyfe Lake. As the time schedule is different for both of the satellites, the images with the smallest time gap were chosen for further investigation. Thus, from five dates, three were approximately 2 days apart, while two images were taken on the same day (**Table 2**).

The methods in this study include both field measurements and remote sensing measurements and techniques (**Figure 3**). The field measurements were performed on 14 June 2018, while the remote sensing data used in the seasonal change analyses were from different months in 2017.

http://dx.doi.org/10.5772/intechopen.80264

Landsat-8	Sentinel-1	Difference
19 February 2017	21 February 2017	~2 days
23 March 2017	23 March 2017	~10 h
27 June 2017	27 June 2017	~10 h
30 August 2017	01 September 2017	~2 days
17 October 2017	19 October 2017	~2 days

Table 2. Satellite data acquisitions over the study area, Seyfe Lake.

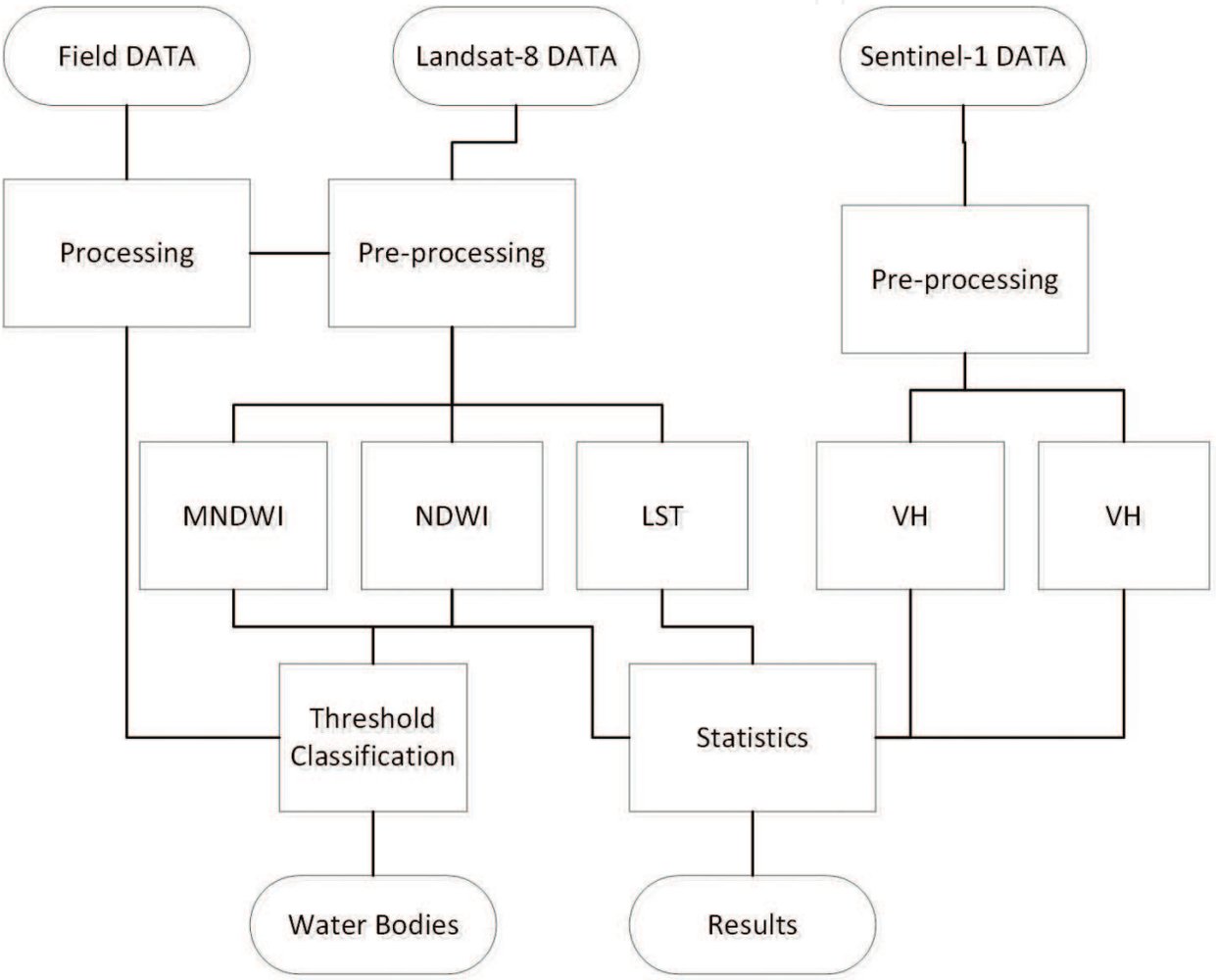

Figure 3. Flowchart of the used methodology.

The field measurements were used for comparison and more accurate classification of the water objects in the study area. Using Landsat 8 satellite data, LST, NDWI, and MNDWI were extracted, and afterward a threshold analysis and classification were made. Sentinel-1 data were preprocessed and the values from the dual polarization data were obtained. The relation between the optical, thermal, and radar satellite data was also investigated. The NDWI, MNDWI, LST, and the dual polarization (VV, VH) values were extracted using approximately

160 random points. The same points were used in all of the satellite images used in this study and were then used for several statistical analyses.

2.2.1. Field measurements

Before going to the field, the availability of satellite imagery was investigated. As the Landsat 8 satellite has a temporal resolution of 16 days, the overpass over the Seyfe Lake was estimated on 14 June 2018. As expected, the overpass happened on 14 June 2018, around 8:20 Coordinated Universal Time (UTC), or around 11:20 local time. The field measurements were taken around 11:00–12:00 local time. At the time of the measurements, the weather was clear, sunny, and hot with a maximum air temperature of 33°C. According to the meteorological records, in the past 2 weeks, three light rains have occurred in the study area, where 3 days before the field measurements, it has rained with over 1 mm (1 kg/m^2).

Several parameters of the study area were taken into consideration during the field measurements: soil moisture, soil texture, soil color, and surface roughness.

The measurements were done 2 km along the study area (**Figure 4**).

According to the field measurements based on the feel of wet soil, the soil at all measurement points can be described as silty clay [35]. The soil moisture observation in the study area showed that three different types of soil can be distinguished: dry soil, moist soil, and wet soil. At the first measurement station (**Figure 4**, detail 1), approximately 3–5 m of the soil can be classified as dry soil with a minimal to no vegetation cover. However, since the spatial resolution of used satellite images, Landsat 8 is 30 m, it is impossible to separate the mentioned dry

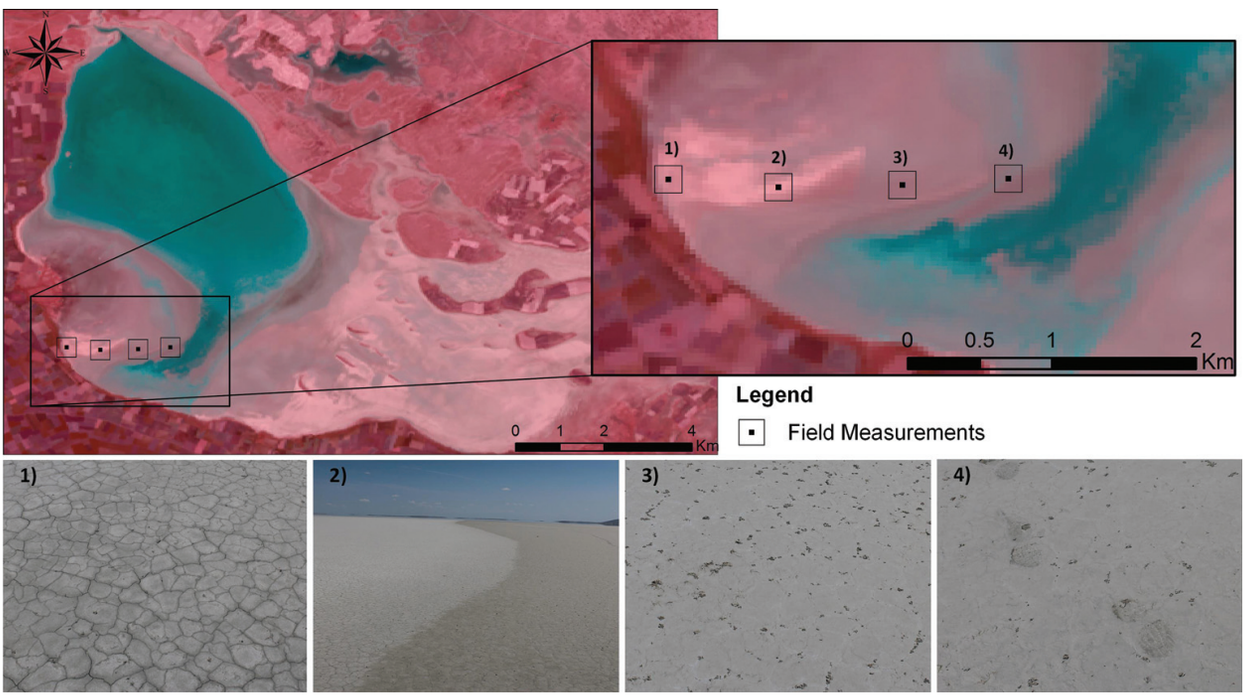

Figure 4. Field measurements details, satellite image (red, green, blue: 6, 3, 4).

http://dx.doi.org/10.5772/intechopen.80264

soil from the further investigated land cover. Further ahead, when touched with hand, the level of moist in the soil could be felt, and the level of moist becomes even higher at the second measurement station, where the difference could be both felt and seen as in **Figure 4**, details 2 and 3. At the fourth measurement station (**Figure 4**, detail 4), the soil was significantly wet, and the field conditions did not allow further investigation/measurements.

2.2.2. NDWI threshold analysis

Using several developed spectral water indices from two or more spectral bands requires an appropriate threshold in order to extract water bodies. The NDWI values range from −1 to +1 where values higher than zero are classified as water bodies. However, with careful adjustment of the NDWI threshold, more accurate results could be achieved [25, 36]. Taking into consideration the field measurements, NDWI threshold analysis on two different water indices was made in order to separate not just the water bodies but also the wetlands in the study area. The first index uses green and near-infrared band (NDWI) [26], while the second band uses green and middle near-infrared band (MNDWI) [27]. In the first case, a threshold value of zero has been set to separate the water bodies from the other land cover features, while in the second case, values close to zero (−0.1 and 0.1) were also set as a threshold value.

2.2.3. LST estimation

With the development of the thermal remote sensing technology, retrieving LST has become the topic for a number of research. A recently developed tool in Erdas Imagine calculates the LST from Landsat 8 satellite data in few steps (**Figure 5**).

First, the top of atmospheric (TOA) spectral radiance (Lλ) is calculated using Eq. (2):

$$L\lambda = M_L * Q_{cal} + A_L - O_i \tag{2}$$

where M_L represents the band-specific multiplicative rescaling factor, Q_{cal} is the value of the thermal band, A_L is the band-specific additive rescaling factor, and O_i is the correction for the thermal band [37]. After the digital numbers (DNs) have been converted to reflection, the data from the thermal band are converted from spectral radiance to brightness temperature (BT) using the thermal constants provided in the metadata file Eq. (3) file (**Table 3**):

$$BT = \frac{K_2}{Ln\left[\left(\frac{K_1}{L\lambda}\right) + 1\right]} - 273.15 \tag{3}$$

Normal difference vegetation index (NDVI) is needed for further calculation of the proportion of vegetation Eq. (4):

$$NDVI = \frac{NIR(band5) - R(band4)}{NIR(band5) + R(band4)} \tag{4}$$

The proportion of vegetation is calculated according to Eq. (4). NDVI values for vegetation and soil ($NDVI_v = 0.5$ and $NDVI_s = 0.2$) are suggested to apply in global conditions [38]:

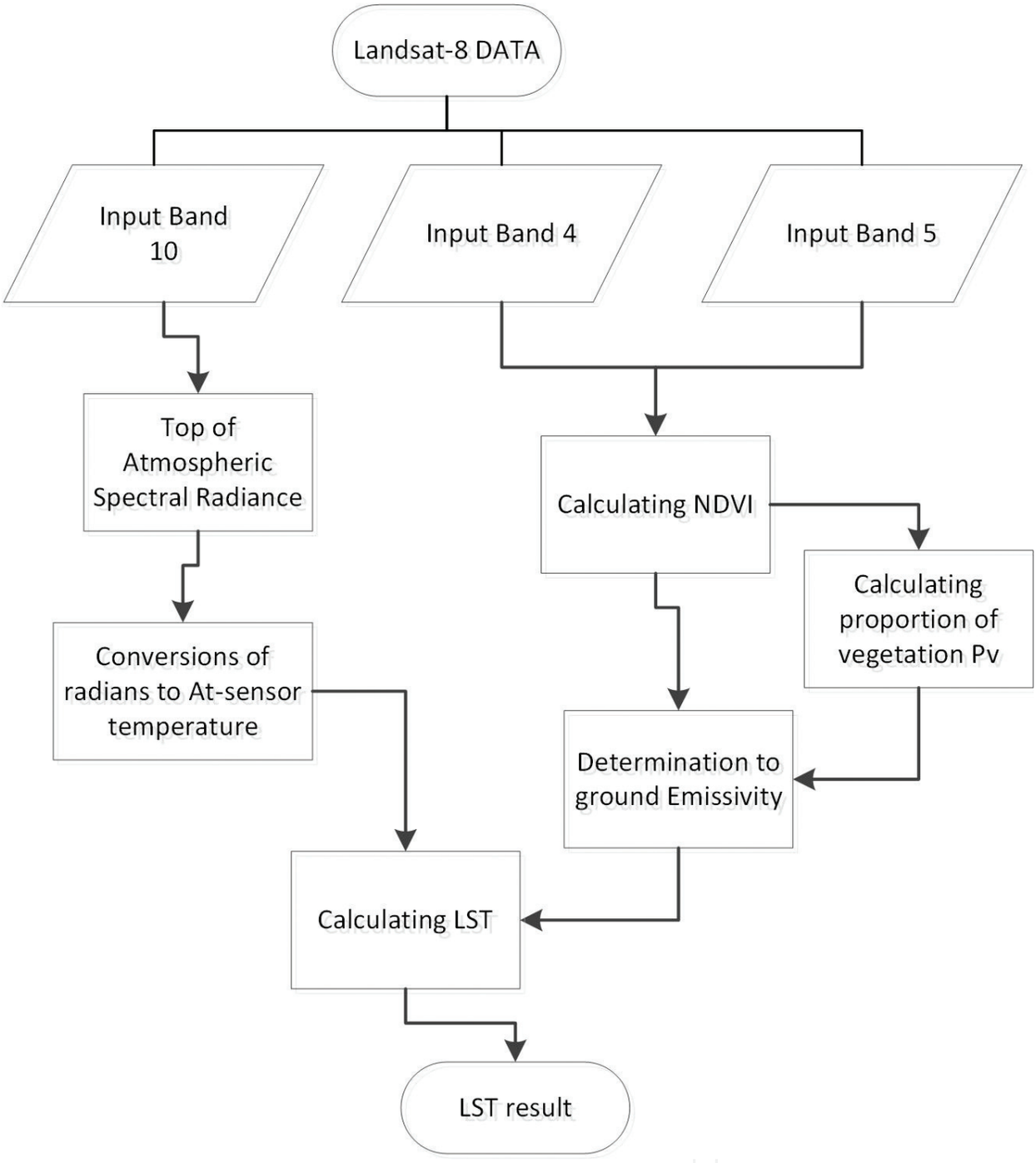

Figure 5. Flowchart of the LST calculation.

$$P_V = \left(\frac{NDVI - NDVI_s}{NDVI_v - NDVI_s}\right)^2 \tag{5}$$

The emissivity can be calculated following Eq. (6):

$$\varepsilon_\lambda = \varepsilon_{v\lambda} P_v + \varepsilon_{s\lambda}(1 - P_v) + C_\lambda \tag{6}$$

where ε_v and ε_s are the vegetation and soil emissivities, respectively, and C represents the surface roughness taken as a constant value of 0.005 [39]. The condition can be represented

Thermal Constant–Band 10	
K1	1321.08
K2	777.89
Rescaling Factor–Band 10	
ML	0.000342
AL	0.1
Correction–Band 10	
Oi	0.29

Table 3. Metadata of Landsat 8 satellite image.

with Eq. (7) where the emissivity constant values are 0.991 for water, 0.962 for built-up areas/bare soil, 0.966 for a mixture of soil and vegetation, and 0.973 for vegetated areas [19]:

$$\varepsilon_\lambda = \begin{cases} \varepsilon_{s\lambda}, & NDVI < NDVI_s \\ \varepsilon_{v\lambda} P_v + \varepsilon_{s\lambda}(1 - P_v) + C, & NDVI_s \leq NDVI \leq NDVI_v \\ \varepsilon_{s\lambda} + C, & NDVI > NDVI_v \end{cases} \quad (7)$$

NDVI values lower than 0 are considered to be water, NDVI values between 0 and 0.2 are considered to be bare soil, and NDVI values between 0.2 and 0.4 are considered to be mixtures of soil and vegetation cover; when the NDVI value is greater than 0.4, it is considered to be covered with vegetation.

The LST or the emissivity-corrected land surface temperature T_s is computed with Eq. (8) [40]:

$$T_s = \frac{BT}{\left\{1 + \left[\frac{\lambda BT}{\rho} ln\, \varepsilon_\lambda\right]\right\}} \quad (8)$$

where Ts is the LST in Celsius, λ is the wavelength of emitted radiance (λ = 10.895) [41], and ρ is a constant calculated with Eq. (9):

$$\rho = h\frac{c}{\sigma}\ (1.438\ x\ 10{-}2\ m\ K) \quad (9)$$

where σ is the Boltzmann constant (1.38 × 10–23 J/K), h is Planck's constant (6.626 × 10–34 J s), and c is the velocity of light (2.998 × 108 ms^{-1}).

3. Results

3.1. Field measurements: NDWI threshold

Comparing the field measurements with remote sensing data, different threshold NDWI and MNDWI values were set for more accurate classification. Since both NIR and SWIR parts of the

electromagnetic spectrum are sensitive to water and wet areas, in this study, both NDWI and MNDWI were considered. The study area, Seyfe Lake contains water area, wetland area, and dry area. The dry area is known to be salt soil [42]. For the threshold value, salt soil areas were not taken into consideration.

As seen in **Figure 6**, the SWIR band is more sensitive to water bodies, as well as to soil moisture. While NIR can only detect the open water bodies, with SWIR beside open water bodies, both shallow water and moist soil can be distinguished from the other land covers.

The higher values of zero thresholds for both NDWI and MNDWI indices indicate water body areas. As seen in **Figure 7**, where the Landsat image is a combination of SWIR, red and green bands, the NDWI threshold results did not classify the shallow water areas as a water body while using the MNDWI successfully extracted both open water bodies and shallow water bodies. However, setting one threshold can only separate the land cover into two classes, in this case, water (NDWI > 0) and other (NDWI < 0), and the wet soils cannot be distinguished from the other land covers. Setting additional threshold values in both NDWI and MNDWI values helped us to distinguish two more classes, shallow water and moist soil, or wetland (**Figures 7** and **8**).

Figure 6. Seyfe Lake: RGB-NIR, red and green (left); RGB-SWIR, red and green (right).

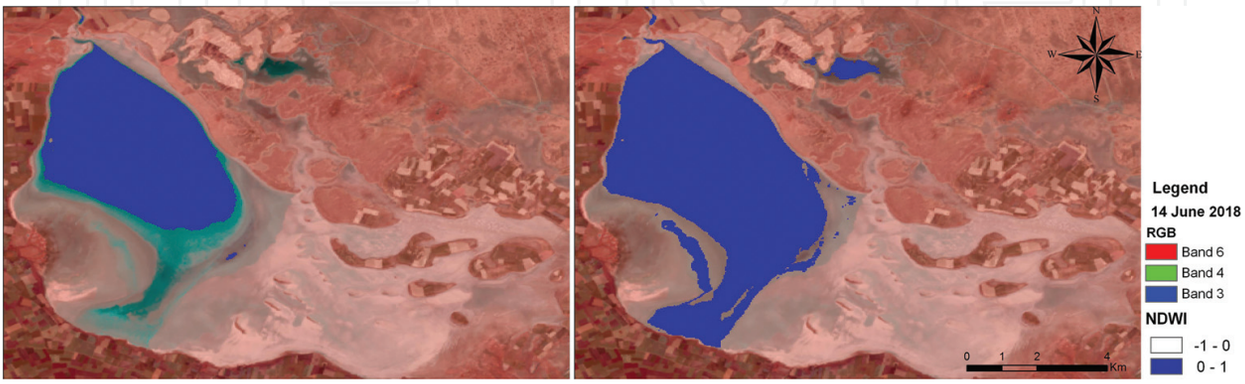

Figure 7. NDWI > 0 (left); MNDWI > 0 (right).

http://dx.doi.org/10.5772/intechopen.80264

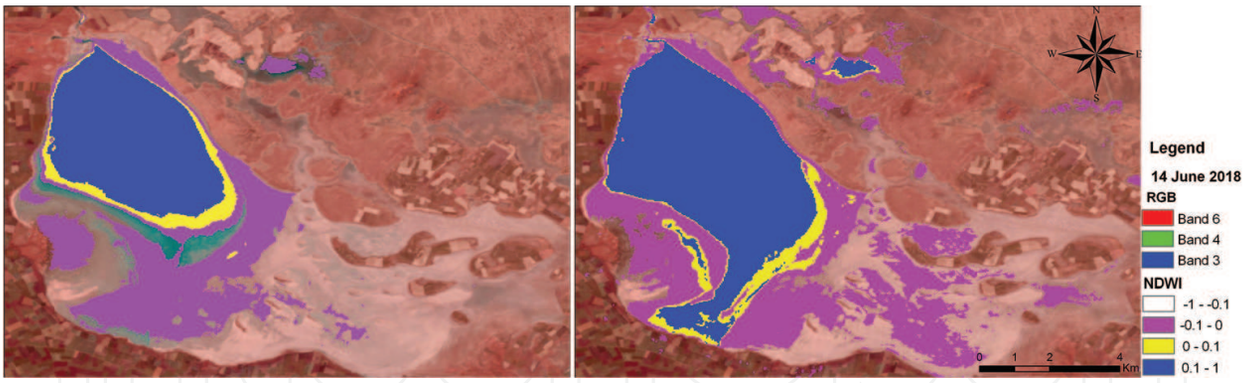

Figure 8. NDWI (left); MNDWI (right).

As it can be seen in **Figures 7** and **8**, the threshold of zero in the NDWI was not successful in extracting shallow water area, while the MNDWI successfully extracted both water object and shallow water areas, but both indices failed in extracting the wet soil within the study area. On the other hand, setting two additional thresholds close to zero (−0.1 and 0.1) showed successful results in distinguishing wetland, shallow water, and water bodies from the other land cover features. In the visual comparison with the field data, the results from the additional thresholds were satisfactorily accurate.

3.2. Seasonal changes

The results from the seasonal changes in the Sefye Lake showed drastic changes over the months. Using both NDWI and MNDWI, according to the field measurements, four classes have been determined, wet soil, salt soil, shallow water, and water. In **Figure 9**, the Sentinel-1, the NDWI classification, and the RGB images from every investigated month are given.

Using the pixel number of every class, the area of each class was calculated, and the results are presented in **Figure 10**. As it can be seen, after March, the water class has decreased for more than 75%, and the area of the shallow water and wet soil has not changed, while the area or the salt soil has significantly increased. The results from August have the highest area of salt soil and the lowest area of water, shallow water, and wet soil, while in October the areas of the salt soil class have decreased, and the areas of the wet soil and shallow water classes have increased. While the water area has been calculated to be more than 20 km^2 in March, in October the water area has been calculated to be 0 km^2.

LST is one of the most important parameters for wetland dynamics (**Figure 11**). The relation between the average LST values and the seasonal changes in Seyfe Lake using NDWI indices has also been investigated. The statistics between these two variables indicates a strong correlation between the LST changes and the changes in every class separately. Thus, the correlation between the wet soil (−0.51), shallow water (−0.58), and water (−0.75) indicates a negative relation, meaning that with the increase of the LST, the values of the mentioned classes decrease. The correlation between the LST and the salt soil has been calculated to be more than 0.8, meaning, with the increase of the LST, the increase of the salt soil (dry soil) area occurs.

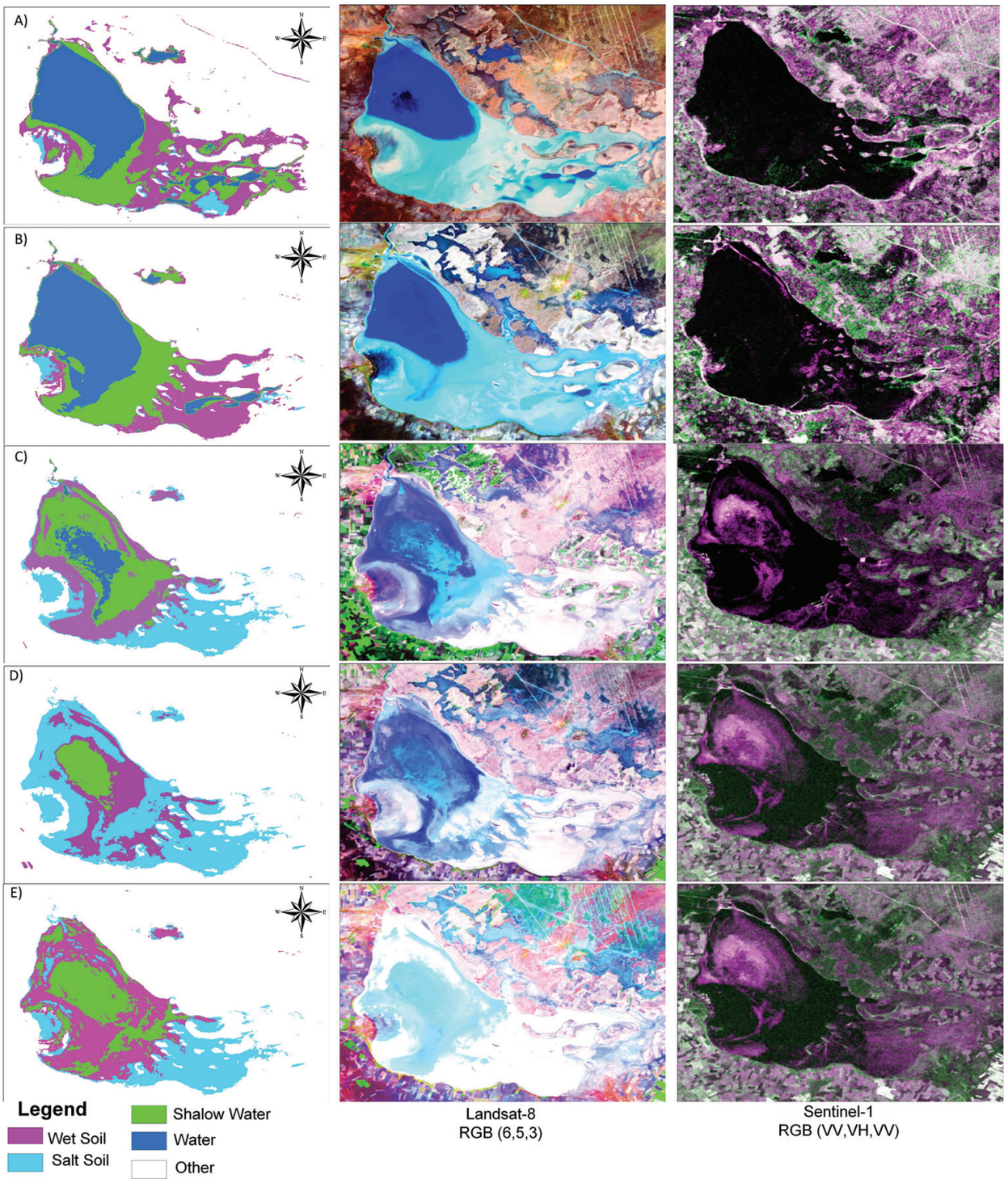

Figure 9. Seasonal wetland dynamic: (A) February, (B) March, (C) June, (D) August, and (E) October.

3.3. Remote sensing data statistics

Using the random point values that were added on the Seyfe Lake area, various statistical analyses were performed in order to find a correlation between the used remote sensing data.

http://dx.doi.org/10.5772/intechopen.80264

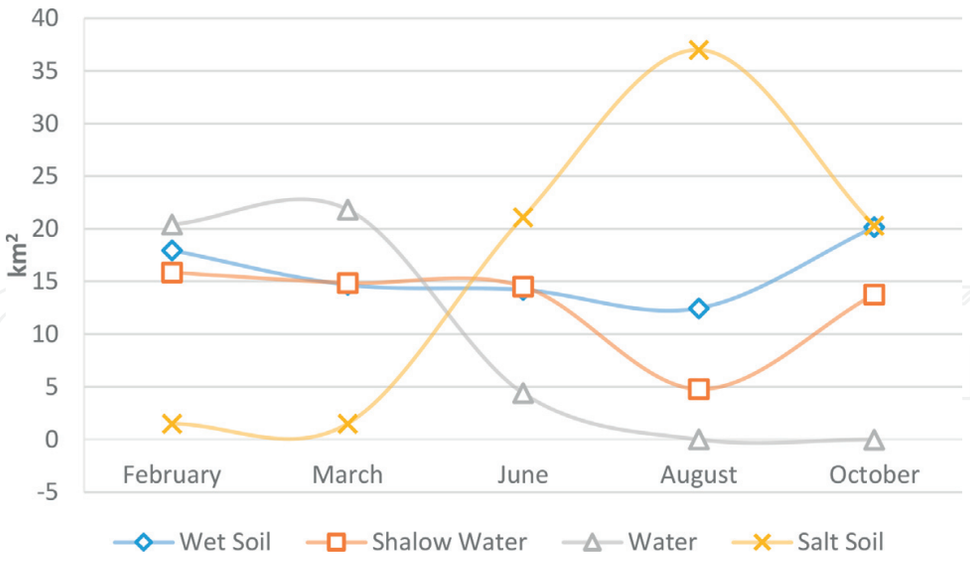

Figure 10. Seasonal Seyfe Lake dynamics.

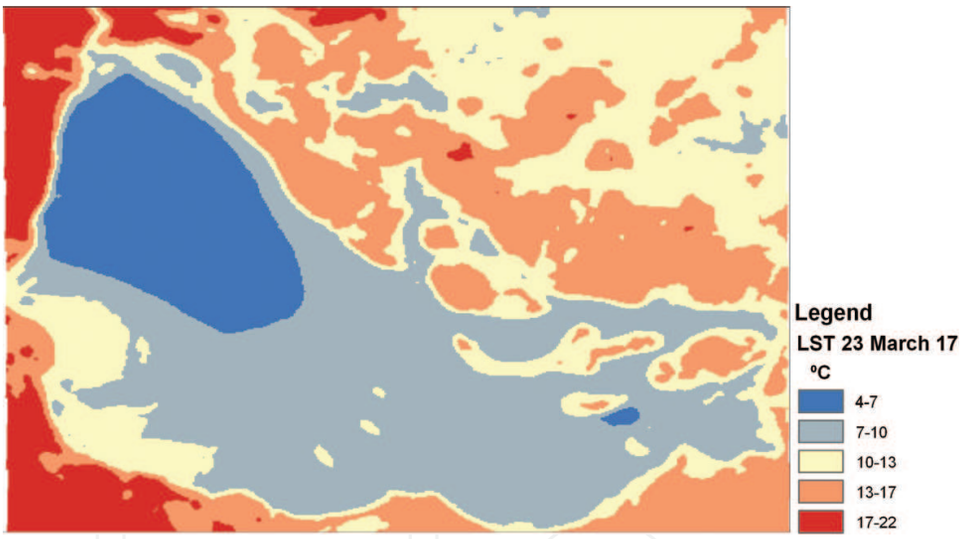

Figure 11. LST results from 23 March 2017.

Thus, the relation between VH, LST, and MNDWI and VV, LST, and MNDWI, between LST and MNDWI, and between VH and VV has been under detailed investigation (**Table 4**).

As seen in **Table 4**, the relation between the investigated parameters has been shown using three different statistical calculations; the multiple R is actually the correlation coefficient between the two variables, and it tells how strong the relationship between these variables is. Values close to 1 indicated a strong relation, while values close to 0 meant no relation at all. R^2, on the other hand, tells us how much of the change in the dependent variable can be explained by the independent variable. The R^2 value can be easily supported with significance variable. So when the significance variable is less than 0.05, the results are significant, or it means that the results did not occur by chance.

	Relation	VH/MNDWI	VH/LST	LST/MNDWI	VV/MNDWI	VV/LST	VV/VH
February	Multiple R	0.445	0.402	0.621	0.429	0.375	0.483
	R square	0.198	0.162	0.385	0.184	0.141	0.233
	Significance F	0.000	0.000	0.000	0.000	0.000	0.000
March	Multiple R	0.321	0.209	0.619	0.065	0.079	0.215
	R square	0.103	0.043	0.383	0.004	0.006	0.046
	Significance F	0.000	0.009	0.000	0.418	0.322	0.007
June	Multiple R	0.100	0.243	0.650	0.196	0.084	0.725
	R square	0.010	0.059	0.422	0.038	0.007	0.525
	Significance F	0.213	0.002	0.000	0.014	0.293	0.000
August	Multiple R	0.218	0.270	0.035	0.242	0.554	0.763
	R square	0.047	0.073	0.001	0.059	0.307	0.582
	Significance F	0.006	0.001	0.000	0.002	0.000	0.000
October	Multiple R	0.311	0.220	0.009	0.429	0.293	0.780
	R square	0.097	0.048	0.000	0.184	0.086	0.609
	Significance F	0.000	0.006	0.907	0.000	0.000	0.000

Table 4. Statistical results.

Since every season has different characteristics, the results were reviewed separately for each month and for each relation. February can be characterized with the lowest LST and high water level. The correlation coefficient between the investigated variables was highest in February for VH-MNDWI, VH-LST, and VV-MDWI. With the assumption that the LST is the independent variable, and the MNDWI is the dependent variable, the R^2 value shows that approximately 39% of the data or the rise of the temperature affects the water area. The results for March were not much different from the results from February with the only difference in the VV-MNDWI and VV-LST relation where the R values were significantly lowered. According to the statistics, the results from June have the most significant value in this study. As seen from the seasonal changes of the Seyfe Lake, in June the MNDWI values showed that the water area has slowly transformed into shallow water and wet soil. In this month the highest correlation coefficient of 0.61 was observed and also the highest R^2 of 0.422. Also, in June, the relation between VV and VH polarization was high with a correlation coefficient of 0.725 and R^2 of 0.52. While the other relation in August and October did not show significant results, the relation between the two polarizations, VV and VH, was noticeable with correlation coefficients higher than 0.76 and R^2 higher than 0.58 in both cases (**Figure 12**).

3.4. Summary

The initial investigation shows a strong relation between the parameters retrieved from the SAR, thermal, and optical satellite data and leads to better understanding of the wetland dynamics. Following the field measurements performed on 14 June 2018, a series of threshold analyses of NDWI and MNDWI were used in order to determine the optimal values for

http://dx.doi.org/10.5772/intechopen.80264

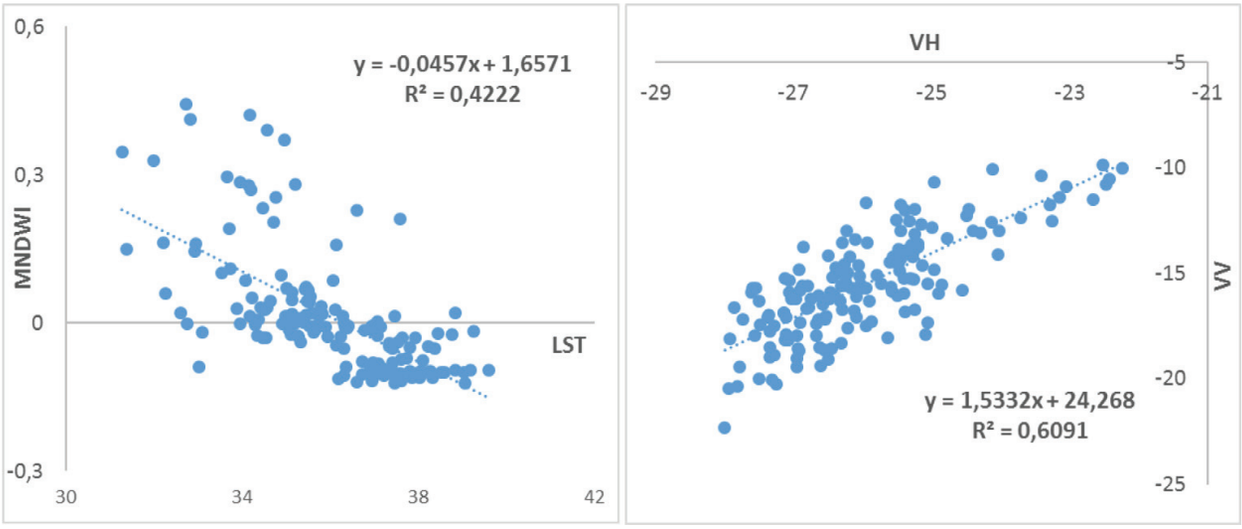

Figure 12. LST-MNDWI relation from June 2017 (left); VV-VH relation from October 2017 (right).

separating water bodies, shallow water, and wet soil from the other land cover classes. It has been concluded that MNDWI performs better in both water and wet soil extraction than NDWI. According to the MNDWI seasonal changes, Seyfe Lake is a very dynamic wetland, and its water area depends on the seasonal temperature. Thus, the water area is inversely proportional to the air temperature. So, for a temporal monitoring of the Lake, in this case, it is recommended to use annual data from the same season/month.

Wetlands ensure critical habitat for wildlife such as migrating water birds. Information gathered from monitoring wetlands may help land managers about the quality of wetlands. Remote sensing data has been the most useful tool to achieve spatial and temporal information about wetlands.

4. Discussion and conclusion

Wetlands are some of the most important ecosystems on Earth if wetlands' function is managed properly which provides tremendous fish and wildlife habitat but also improves groundwater quality and natural floodwater control. Global climate change and anthropogenic impact degrade wetlands, which creates a serious problem in identifying and quantifying wetland areas. Consequently, it is critical to be able to assess the status and quality of our remaining wetlands.

Remote sensing is a major source of spatial information about the land cover. Although a number of studies have investigated the relation between SAR and optical sensors in different land classes, the relation between backscatter values, NDWI, and LST values in wetland classes has not been a subject of a delicate investigation. In this chapter we investigate the relation between several remote sensing parameters, from a different aspect, trying to find a significant relation that will explain the wetland dynamics for better mapping, monitoring, and managing of wetland areas. The results in this study show a strong relation between the investigated

variables. However, while some variables have strong relation when the water area is high, others have stronger relation when the lake is completely dried. The results of the statistical analyses from the month of June were taken to be highly significant from two points of view; the correlation between LST and MNDWI was more than 0.65, while the R^2 was more than 0.42. Taking in consideration the relation between the average temperature from each month and the area of each class, it can be concluded that with a correlation of −0.75, the water area depends on the temperature, or as the temperature increases, the water area decreases.

As stated in previous studies, with careful adjustment of the NDWI threshold, more accurate results could be achieved [25, 36]. Thus, it can be concluded that the values close to zero in the MNDWI threshold can give valuable information about the soil moisture. The positive values close to zero (0.1) indicate the shallow water areas, while the negative values close to zero (−0.1) indicate wet soil.

Even though in more of the cases the relation between the Landsat 8 and the Sentinel-1 parameters was high, in some cases their correlation was close to zero. Thus, while the changes of the VH values in March could be explained about 20% with the help of LST, the VV values could be explained about 20% with the help of MNDWI in October. The relation between the two polarization has highest values when the water level is at its lowest level because at that time the study area is mostly covered with dry soil. For a better understanding of wetland dynamics, we recommend using new techniques and different data fusion for exploring the full potential of remote sensing in wetland monitoring, supported with field measurements.

Acknowledgements

The authors want to thank Onur Kaplan for his contribution during the field measurements. This chapter was supported and funded by Anadolu University Scientific Research Projects Commission under the Grant No. 1705F121.

Conflict of interest

The authors declare no conflict of interest.

Author details

Gordana Kaplan[1]*, Zehra Yigit Avdan[2] and Ugur Avdan[1]

*Address all correspondence to: kaplangorde@gmail.com

1 Earth and Space Sciences Institute, Eskisehir Technical University, Eskisehir, Turkey

2 Department of Environmental Engineering, Eskisehir Technical University, Eskisehir, Turkey

References

[1] Ustin S. Manual of Remote Sensing: Remote Sensing for Natural Resource Management and Environmental Monitoring. Hoboken, NJ: Wiley; 2004

[2] Czajkowski K, Torbick N, Lawrence P. Application and assessment of a GIScience model for jurisdictional wetlands identification in Northwestern Ohio. In: Wetland and Water Resource Modeling and Assessment: A Watershed Perspective. CRC Press; 2007. pp. 2-12

[3] Schmidt K, Skidmore A. Spectral discrimination of vegetation types in a coastal wetland. Remote Sensing of Environment. 2003;**85**(1):92-108

[4] Kaplan G, Avdan U. Mapping and monitoring wetlands using Sentinel-2 satellite imagery. In: ISPRS Annals of Photogrammetry, Remote Sensing and Spatial Information Sciences; 2017. pp. 271-277

[5] Kaplan G, Avdan U, Avdan ZY. Estimation of wetland biomass using Sentinel-2 Images. Icocce Capadokia, Nevsehir, Turkey: Digital Proceeding of ICOCEE; May 2017

[6] Gorham E. Northern peatlands: Role in the carbon cycle and probable responses to climatic warming. Ecological Applications. 1991;**1**(2):182-195

[7] Guo M, Li J, Sheng C, Xu J, Wu L. A review of wetland remote sensing. Sensors. 2017;**17**(4): 777

[8] Zhang S, Na X, Kong B, Wang Z, Jiang H, Yu H, et al. Identifying wetland change in China's Sanjiang Plain using remote sensing. Wetlands. 2009;**29**(1):302-313

[9] Jones JW. Efficient wetland surface water detection and monitoring via landsat: Comparison with in situ data from the everglades depth estimation network. Remote Sensing. 2015;**7**(9):12503-12538

[10] Baker C, Lawrence RL, Montagne C, Patten D. Change detection of wetland ecosystems using Landsat imagery and change vector analysis. Wetlands. 2007;**27**(3):610-619

[11] Frohn RC, Reif M, Lane C, Autrey B. Satellite remote sensing of isolated wetlands using object-oriented classification of Landsat-7 data. Wetlands. 2009;**29**(3):931-941

[12] Cazals C, Rapinel S, Frison P, Bonis A, Mercier G, Mallet C, et al. Mapping and characterization of hydrological dynamics in a coastal marsh using high temporal resolution Sentinel-1A images. Remote Sensing. 2016;**8**:570

[13] Muro J, Canty M, Conradsen K, Hüttich C, Nielsen AA, Skriver H, et al. Short-term change detection in wetlands using Sentinel-1 time series. Remote Sensing. 2016;**8**(10):795

[14] Dabrowska-Zielinska K, Budzynska M, Tomaszewska M, Malinska A, Gatkowska M, Bartold M, et al. Assessment of carbon flux and soil moisture in wetlands applying Sentinel-1 data. Remote Sensing. 2016;**8**(9):756

[15] Kaplan G, Avdan U. Sentinel-1 and Sentinel-2 data fusion for wetlands mapping: Balikdami, Turkey. In: International Archives of the Photogrammetry, Remote Sensing & Spatial Information Sciences. Vol. 42, Issue 3; 2018

[16] El-Shirbeny M, Abutaleb K. Sentenel-1 radar data assessment to estimate crops water stress. Technology. 2017;**5**:47-56

[17] Muro J, Heinmann S, Strauch A, Menz G, editors. Land surface temperature retrieval in wetlands using normalized difference vegetation index-emissivity estimation and ASTER emissivity product. In: Living Planet Symposium; 2016

[18] Mira M, Ninyerola M, Batalla M, Pesquer L, Pons X. Improving mean minimum and maximum month-to-month air temperature surfaces using satellite-derived land surface temperature. Remote Sensing. 2017;**9**(12):1313

[19] Wang F, Qin ZH, Song CY, Tu LL, Karnieli A, Zhao SH. An improved mono-window algorithm for land surface temperature retrieval from Landsat 8 thermal infrared sensor data. Remote Sensing. 2015;**7**(4):4268-4289

[20] Avdan U, Jovanovska G. Algorithm for automated mapping of land surface temperature using LANDSAT 8 satellite data. Journal of Sensors. 2016;**2016**

[21] Yuan F, Bauer ME. Comparison of impervious surface area and normalized difference vegetation index as indicators of surface urban heat island effects in Landsat imagery. Remote Sensing of Environment. 2007;**106**(3):375-386

[22] Kaplan G, Avdan U. 2013 Balochistan Earthquakes Thermal Anomalies. 4th ICEES: Eskisehir, Turkey; October 2017

[23] Kaplan G, Avdan U. Water extraction technique in mountainous areas from satellite images. Journal of Applied Remote Sensing. 2017;**11**(4):046002

[24] Eisavi V, Yazdi AM, Niknezhad SA. Spatial and temporal modeling of wetland surface temperature using Landsat-8 imageries in Sulduz, Iran. Journal of the Faculty of Forestry Istanbul University. İstanbul Üniversitesi Orman Fakültesi Dergisi. 2016;**66**(1):46-58

[25] Gao B-C. NDWI—A normalized difference water index for remote sensing of vegetation liquid water from space. Remote Sensing of Environment. 1996;**58**(3):257-266

[26] McFeeters SK. The use of the normalized difference water index (NDWI) in the delineation of open water features. International Journal of Remote Sensing. 1996;**17**(7):1425-1432

[27] Xu H. Modification of normalised difference water index (NDWI) to enhance open water features in remotely sensed imagery. International Journal of Remote Sensing. 2006;**27**(14): 3025-3033

[28] Mitsch WJ, Gosselink JG. Wetlands. Wetlands. 5th edition. 2015:155-204

[29] Adam E, Mutanga O, Rugege D. Multispectral and hyperspectral remote sensing for identification and mapping of wetland vegetation: A review. Wetlands Ecology and Management. 2010;**18**(3):281-296

[30] Barsi JA, Lee K, Kvaran G, Markham BL, Pedelty JA. The spectral response of the Landsat-8 operational land imager. Remote Sensing. 2014;**6**(10):10232-10251

[31] Attema E, Davidson M, Floury N, Levrini G, Rosich B, Rommen B, et al., editors. Sentinel-1 ESA's new European radar observatory. In: 2008 7th European Conference on Synthetic Aperture Radar (EUSAR). VDE; 2008

[32] Torres R, Snoeij P, Geudtner D, Bibby D, Davidson M, Attema E, et al. GMES Sentinel-1 mission. Remote Sensing of Environment. 2012;**120**:9-24

[33] Richards JA. Remote sensing with imaging radar. Berlin: Springer; Oct 8, 2009

[34] European Space Agency (20 November 2017), Tutorials; Retrived from: https://earth.esa.int/web/sentinel/toolboxes/sentinel-1/tutorials

[35] McCoy RM. Field Methods in Remote Sensing. Guilford Press; 2005

[36] Ji L, Zhang L, Wylie B. Analysis of dynamic thresholds for the normalized difference water index. Photogrammetric Engineering & Remote Sensing. 2009;**75**(11):1307-1317

[37] Barsi JA, Schott JR, Hook SJ, Raqueno NG, Markham BL, Radocinski RG. Landsat-8 thermal infrared sensor (TIRS) vicarious radiometric calibration. Remote Sensing. 2014; **6**(11):11607-11626

[38] Sobrino JA, Jimenez-Munoz JC, Paolini L. Land surface temperature retrieval from LANDSAT TM 5. Remote Sensing of Environment. 2004;**90**(4):434-440

[39] Sobrino JA, Raissouni N. Toward remote sensing methods for land cover dynamic monitoring: Application to Morocco. International Journal of Remote Sensing. 2000;**21**(2):353-366

[40] Stathopoulou M, Cartalis C. Daytime urban heat islands from Landsat ETM+ and Corine land cover data: An application to major cities in Greece. Solar Energy. 2007;**81**(3):358-368

[41] Markham BL, Barker JL. Spectral characterization of the Landsat thematic mapper sensors. International Journal of Remote Sensing. 1985;**6**(5):697-716

[42] Reis S, Yilmaz HM. Temporal monitoring of water level changes in Seyfe Lake using remote sensing. Hydrological Processes. 2008;**22**(22):4448-4454

IntechOpen